# Intra- and Inter-Modality Registration

for

# Validation of MRI based Hypoxia Imaging

by

Sulagna Sahu

A Thesis Presented in Partial Fulfillment
of the Requirements for the Degree
Master of Science

Approved June 2018 by the
Graduate Supervisory Committee:

Vikram Kodibagkar, Chair
Rosalind Sadleir
Barbara Smith

ARIZONA STATE UNIVERSITY

August 2018

# ABSTRACT

Hypoxia is a pathophysiological condition which results from lack of oxygen supply in tumors. The assessment of tumor hypoxia and its response to therapies can provide guidelines for optimization and personalization of therapeutic protocols for better treatment. Previous research has shown the difficulty in measuring hypoxia anatomically due to its heterogenous nature. This makes the study of hypoxia through various imaging modalities and mapping techniques crucial. The potential of hypoxia targeting $T_1$ contrast agent GdDO3NI in generating hypoxia maps has been studied earlier. In this work, the similarities between hypoxia maps generated by MRI using GdDO3NI and pimonidazole based immunohistochemistry (IHC) in non-small cell lung carcinoma bearing mice have been studied. Six NCI-H1975 tumor-bearing mice were studied. All animal studies were approved by Arizona State University's Institute of Animal Care and Use Committee (IACUC). Post co-injection of GdDO3NI and pimonidazole, $T_1$ weighted 3D gradient echo MR images were acquired. For *ex-vivo* analysis of hypoxia, 30 μm thick tumor sections were obtained for each harvested tumor and were stained for pimonidazole and counter-stained with DAPI for nuclear staining. Pimonidazole (PIMO) is clinically used as a "gold standard" hypoxia marker. The key process involved stacking and iterative registration based on quality metric SSIM (Structural Similarity) Index of DAPI stained images of 5 consecutive tumor sections to produce a 3D volume stack of 150 μm thickness. Information from the 3D volume is combined to produce one final slide by averaging. The same registration transform was applied to stack the pimonidazole images which were previously thresholded to highlight hypoxic regions. The registered IHC stack was then co-registered with a single thresholded $T_1$ weighted gradient echo MRI slice of the same location (~156

μm thick) using an elastic B-splines transform. The same transform was applied to achieve the co-registration of pimonidazole and MR percentage enhancement image. Image similarity index after the co-registration was found to be greater than 0.5 for 5 of the animals suggesting good correlation. $R^2$ values were calculated for both hypoxic regions as well as tumor boundaries. All the tumors showed a high boundary correlation value of $R^2$ greater than 0.8. Half of the animals showed high $R^2$ values greater than 0.5 for hypoxic fractions. The RMSE values for the co-registration of all the animals were found to be low further suggesting better correspondence and validating the MR based hypoxia imaging.

# ACKNOWLEDGMENTS

Throughout my time at ASU as a master's student, I have had a lot of people to be thankful to. First and foremost, I would like to thank Dr. Vikram Kodibagkar, my thesis advisor, for his knowledgeable guidance and support. I am grateful to my thesis committee members Dr. Rosalind Sadleir and Dr. Barbara Smith for finding time to review my research work. I am extremely grateful to everyone associated with ProBE Lab, specially, Dr. Shubhangi Agarwal, Carlos Renteria, Babak Moghdas, Nutandev Bikkamane and John Tobey for all their help. I would like to thank Laura Hawes, our academic advisor for being incredibly patient and helpful with paperwork. My friends at ASU have helped keep the motivation alive and I am appreciative of their presence in my life. I appreciate the efforts put in by software developers who have created MATLAB and ImageJ, the main tools for my whole project. Last but not the least, my family deserves applause and gratitude for their unconditional love and support.

TABLE OF CONTENTS

LIST OF FIGURES ..... vi

CHAPTER

1. INTRODUCTION ..... 1

1.1 CANCER AND SIGNIFICANCE OF TUMOR HYPOXIA ..... 1
1.2 CURRENT HYPOXIA IMAGING TECHNIQUES ..... 2
1.3 PREVIOUS WORK ..... 3
1.4 IMAGE REGISTRATION ..... 5

2. MATERIALS AND METHODS ..... 9

2.1 INTER MODALITY REGISTRATION OF HISTOLOGY SECTIONS ..... 9
2.1.1 ROI Selection and Sampling ..... 9
2.1.2 Histogram Equalization: ..... 10
2.1.3 Thresholding of PIMO Images and PIMO Hypoxic Fraction ..... 11
2.2 MULTI MODALITY IMAGE REGISTRATION ..... 14
2.2.1 Pre-Processing before Co-Registration. ..... 14
2.2.2 Boundary Landmark Selection for Registration ..... 18
2.2.3 Structural Similarity (SSIM) Index ..... 19
2.2.4 Selection of Final MR Image Slice and Registered PIMO Image ..... 20
2.2.5 Coefficient of Determination and Root Mean Square Error ..... 21
2.2.6 Statistical Analysis ..... 21

3. RESULTS ..... 22

3.1 Hypoxic Fraction Analysis ..... 22
3.2 Comparison of Registration Metrics ..... 24

3.3 Visualization of Intra Modality Registration..... 25
3.4 Visualization of Inter Modality Registration..... 26
CONCLUSION ..... 28
FUTURE WORK ..... 29
REFERENCES .....30

LIST OF FIGURES

Figure 1 Graph showing results from an experiment done by J. Martin Brown et. Al to see the response to radiation therapy in different levels of oxygen saturation [4]. ..... 2

Figure 2 Description of imaging protocol used previously [14]. ..... 5

Figure 3 An example of registration methodology used by David Pilutti et al. to apply to DCE MRI. (a) is the fixed image (b) is the moving image (c) is the registered image (d) is the ROI mask and (e) and (f) show checkerboard view of (a) and (b) before and after registration. ..... 6

Figure 4 ROI selection to remove background noise..... 10

Figure 5 The first row shows a set of input images having intensity variations. The second row shows the same set after histogram equalization. The input image set now has consistent intensity range. ..... 11

Figure 6 Input DAPI image before (a) and after (b) thresholding. ..... 12

Figure 7 Representation of working algorithm for intra-modality registration. (1) is the first fixed image and (2) is the first moving image. ..... 14

Figure 8 Input T1 weighted gradient echo MR image (b) after segmentation is done to keep tumor region of interest. ..... 15

Figure 9 Input MR percentage enhancement image before (a) and after (b) thresholding. ..... 16

Figure 10 Overlay images of MR images at first and last time point of acquisition before (a) and after (b) motion correction for axial view orientation. ..... 17

Figure 11 Checkerboard display of MR images of one tumor before (left-hand side image) and after (right-hand side image) motion correction shown in 3 directions to represent 3D motion. ..... 18
Figure 12 Landmark selection on MR ROI and DAPI ROI for correspondence..... 18
Figure 13 Yellow lines on (a) represent transformation followed after landmark selection to obtain a final registered PIMO image in (b). ..... 19
Figure 14 The first figure shows a selected a selected MR slice for one tumor and (1) and (2) show two different PIMO registered and stacked images to compare with MRI. ..... 21
Figure 15 Scatter plot for hypoxia fractions for all 6 tumors. X axis represents PIMO hypoxic fraction and Y axis represents MR hypoxic fraction. Shaded area represents 95% confidence interval range. ..... 23
Figure 16 Scatter plot for hypoxia fractions for all 5 tumors (excluding oulier). X axis represents PIMO hypoxic fraction and Y axis represents MR hypoxic fraction. Shaded area represents 95% confidence interval range. ..... 24
Figure 17 Intra-modality registration results. (a) Registered DAPI stained image stack and (b) Registered pimonidazole image stack for the first animal. 3D visualization of registered DAPI stack shown in grayscale in (c) shows consistent boundary outline between the histology sections..... 25
Figure 18 Representation of inter-modality registration of MR and Histology for the six tumors. First column shows thresholded MR percentage enhancement image and second column shows pimonidazole image generated after co-registration. ..... 26

Figure 19 Left-hand image shows checkerboard view after co-registration for the six tumors. Right-hand image in each case shows ROI boundaries on the final registered PIMO image. ..... 27

# CHAPTER 1

# INTRODUCTION

## 1.1 CANCER AND SIGNIFICANCE OF TUMOR HYPOXIA

Cancer is a deadly disease in which a group of abnormal cells divide and multiply uncontrollably. Metastatic cancerous growth has the potential to spread and invade to various parts of the body. Cancer disrupts lifestyles and results in death often. Various research and surveys have shown that by 2015 almost 90.5 million people were affected by over 100 different types of cancer [1]. Most of the malignant cancers excepting leukemia form solid tumors. In solid tumors, hypoxia is a condition resulting from lack of oxygen supply due to rapid consumption of oxygen by proliferating cancer cells. Due to excessive cell density, diffusion distance between oxygen rich blood vessels and cells increases and transport capacity of blood reduces due to presence of disease related anemia [2]. Hypoxia decreases the efficiency of radiotherapy and anticancer chemotherapy. Tumors have a median partial pressure of oxygen at around 10 mmHg as opposed to normal tissue which have oxygen partial pressures in the range of 40-60 mmHg. Hypoxic cells become resistant to radiotherapy through HIF-1 (Hypoxia Inducible Factor 1) mediated mechanisms. Studies show that higher levels of oxygen promote the damage caused by radiotherapy owing to the fact that oxygen combines with the free radical produced by ionization [3][4]. Due to larger diffusion distances and lower diffusion rates it gets more difficult for chemotherapy drugs to reach hypoxic cells [5]. Chemotherapy studies have shown that hypoxia leads to the upregulation of drug resistant genes like p-glycoprotein [6] and the decrease in oxygen level reduces the cytotoxic DNA lesions caused in tumorous cells [4].

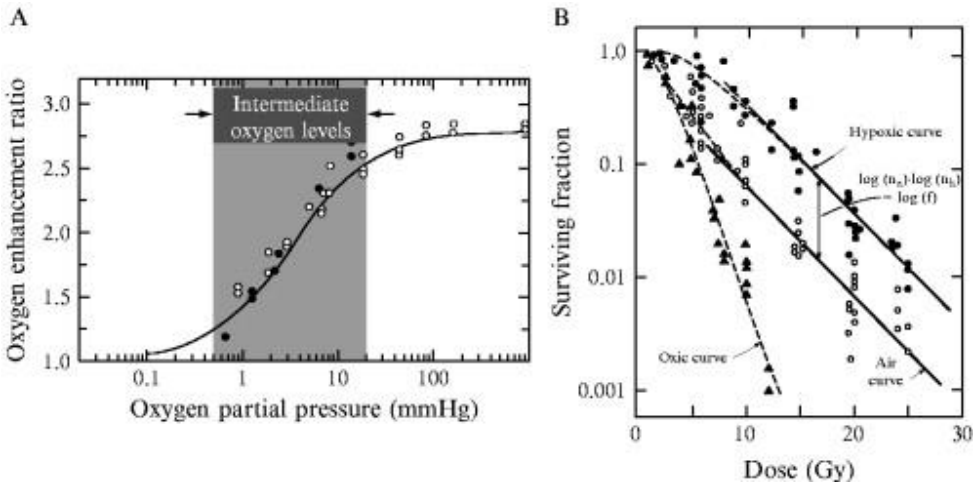


Figure 1 Graph showing results from an experiment done by J. Martin Brown et. Al to see the response to radiation therapy in different levels of oxygen saturation [4].

This makes study and imaging of hypoxia extremely important. Localization of hypoxia helps in targeted therapies for example delivering hypoxia-selective cytotoxins/drugs, and HIF-1 inhibitors and booster radiation dose to hypoxia specific regions of the tumor in a therapy called SIB-IMRT (simultaneous integrated boost intensity-modulated radiation therapy) [3].

## 1.2 CURRENT HYPOXIA IMAGING TECHNIQUES

Some of the direct techniques used to image hypoxia include invasive injection of oxygen probes, phosphorescence quenching and 19F magnetic resonance spectroscopy. These techniques are invasive and/or have limited depth of view in imaging hypoxia. To overcome this many efficient in vivo methods of imaging have been developed like use of endogenous markers like glucose transporter 1, HIF 1 and Osteopontin [7]. Physiological methods like BOLD MRI, photoacoustic tomography, near-infrared spectroscopy, immunohistology and PET imaging have also been studied to detect and

image hypoxia. MR contrast agents like [$^{18}$F]fluoromisonidazole, [$^{18}$F]fluoroerythronitroimidazole, copper-64 diacetyl-bis($N^4$ - methylthiosemicarbazone), etc. used for imaging hypoxia exploits the principle of selective enzyme-mediated reduction of the nitro group in 2-nitroimidazole-containing compounds under hypoxic conditions [8][9]. The hypoxia targeting ability of a gadolinium tetraazacyclododecanetetraacetic acid monoamide conjugate of 2-nitroimidazole (GdDO3NI) has been validated previously in-vitro using 9L glioma cells incubated under hypoxia and AT1 xenograft models respectively [10]. *Ex vivo* methods of assessing tumor hypoxia include immunohistochemical staining for either intrinsic markers of hypoxia or externally injected nitroimidazoles adducts. Pimonidazole targets hypoxic cells by binding to thiol-containing proteins and gets detected by using a mouse monoclonal antibody [11]. Pimonidazole is currently the 'gold standard' for measuring hypoxia *ex vivo*. Both electrode and immunohistochemical assessments are invasive. In immunohistological staining, unless whole-tumor mounts are used, tumors need to be harvested and sectioned and will provide a limited sample and have cutting and distortion artifacts due to sectioning. Hence, combination study of two different modalities of imaging can give interesting results.

## 1.3 PREVIOUS WORK

GdDO3NI has great potentials for non-invasive longitudinal study and imaging of hypoxia. Previously in ProBE Lab, GdDO3NI has been used to generate three-dimensional maps to study degree and distribution of hypoxia before and after administration of hypoxia activated therapy. Six different NCI-H1975 tumor-bearing

mice were studied. All animal studies were approved by Arizona State University's Institute of Animal Care and Use Committee (IACUC) and were performed in accordance with the relevant guidelines. The mice were co-injected with 0.3 mmole\kg body weight GdDO3NI and 60 mg/kg pimonidazole. The tumors were ready for imaging when they reached ~300 mm3 in volume. $T_1$ weighted 3D gradient echo MR images with an isotropic resolution of ~156 μm, a TE of 3 ms, TR of 80 ms and an alpha of 35º (FOV= 2 cm × 2 cm × 2 cm, matrix=128 × 64 × 64 reconstructed to 128 x 128 x 128) were acquired for *in-vivo* analysis. One 3D gradient echo image was acquired pre-injection and two 3D gradient echo images were acquired at 60 min and 125 min post-GdDO3NI injection. For ex-vivo analysis of hypoxia, 30 μm thick tumor sections (30 sections) at the same imaging plane as MR were obtained using a cryostat. The tumor sections were stained with FITC conjugated anti-pimonidazole antibody and counterstained with DAPI (4′,6-diamidino-2-phenylindole) for nuclear staining. The stained sections were mounted with Vectashield medium (Vector Laboratories, Burlingame, CA) and visualized under the DMI 6000B Leica Microsystems microscope using the green channel for pimonidazole and the blue channel for DAPI at 5X magnification. Pimonidazole is clinically used as a "gold standard" hypoxia marker and is ideal for comparison. GdDO3NI successfully reported the baseline distribution and intensity of hypoxia in non-small cell lung cancer models (NCI-H1975). A response to the hypoxia activated prodrug tirapazamine (TPZ) was also studied. Heterogeneous distribution of hypoxia was found within all the NSCLC tumors. A significant decrease in tumor growth as compared to the untreated control was observed in TPZ treated tumors. Various other studies have shown that effective

TPZ treatment results in vascular shutdown in tumors, resulting in increased hypoxia in the central regions of the tumors [12][13].

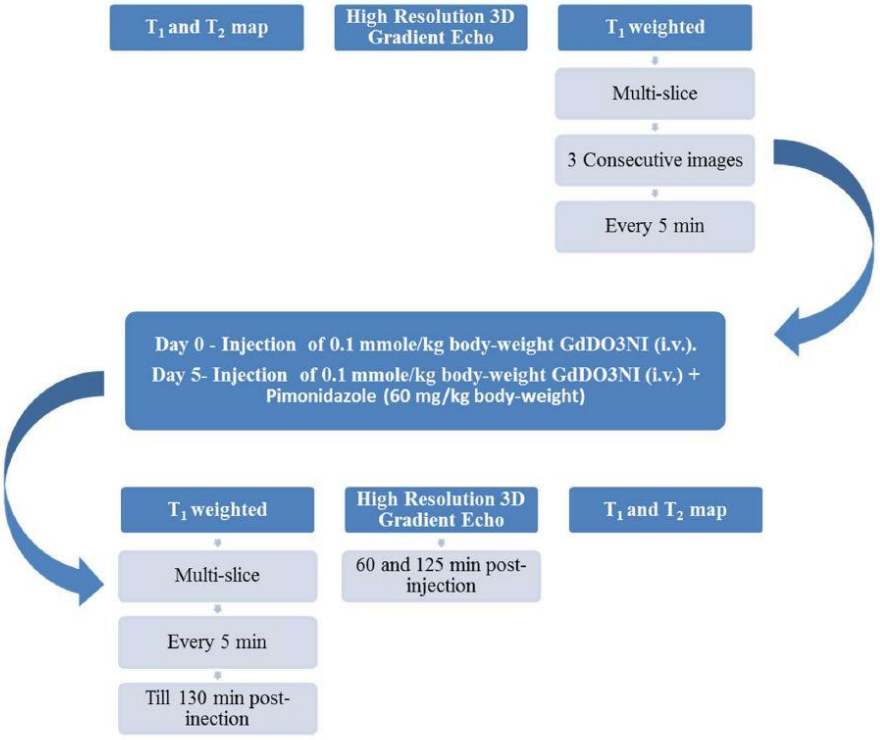


Figure 2 Description of imaging protocol used previously [14].

## 1.4 IMAGE REGISTRATION

Conventional *in vivo* diagnostic imaging techniques have been helpful for the detection of hypoxia in tumor, but with advancement of different techniques to increase the sensitivity and specificity of tumor information provided, the need to combine information provided by different modalities is paving a path towards in vivo imaging without the need for invasive techniques. Image registration is a technique to compare information visible on multiple images. It aligns multiple images into one scene to produce a final fused image representing information from all the input images. Histology staining techniques show the ground truth information and can be used to

compare with the spatial distribution represented by MR images. Figure 3 show an example of registration used on DCE MRI for abdominal tumors [15]. Previously, research has been done for better detection of prostate tumor by multi-modality registration of histology with ultrasound and MRI [16][17].

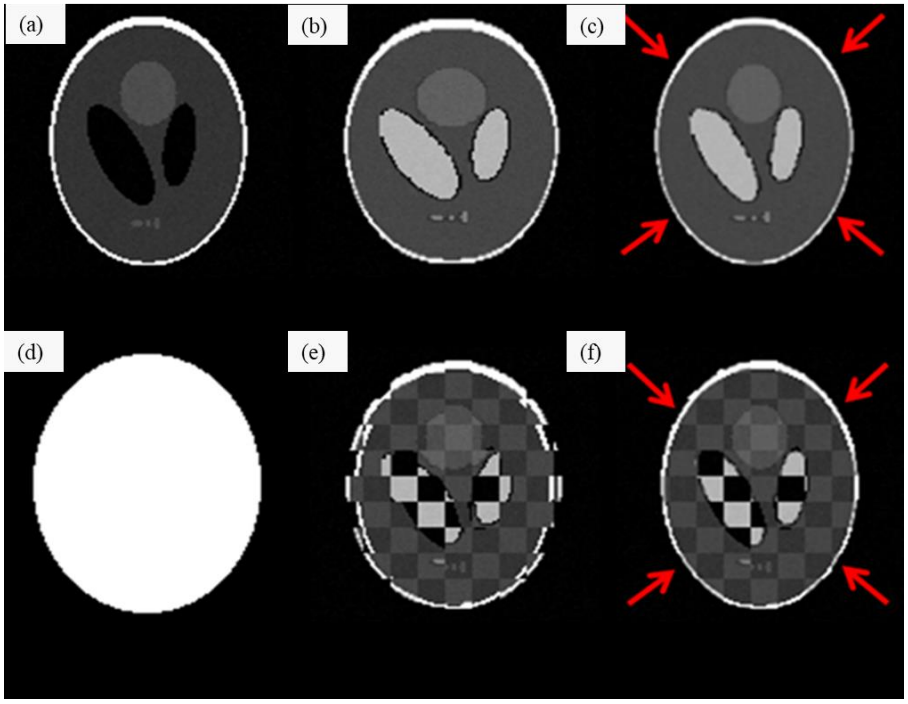


Figure 3 An example of registration methodology used by David Pilutti to apply to DCE MRI. (a) is the fixed image (b) is the moving image (c) registered image (d) is the ROI mask and (e) and (f) show checkerboard of (a) and (b) before and after registration.

Very few studies have been done to study hypoxia through multi-modality registration. Comparing spatial correspondence between MRI and histology provides information about MRI's capability to characterize hypoxia in tumor and underlying pathophysiology. Comparison with histology is particularly challenging because of

deformations that happen through the process. For final histological sections the tumor tissue is excised, fixed by formalin and dehydrated followed by embedding in paraffin, sectioning, and rehydration to get staining. This causes significant tissue deformation which also changes tumor appearance. Difference in slice thickness in different modalities and motion artifacts also pose additional challenges. There are inherent differences in intensity patterns generated as histology is in color and MRI is grayscale. Although rigid body registration and affine registration are good in aligning shape and structure of tumors they cannot account for non-linear deformation and stretching in internal patterns. To overcome this elastic registration techniques, must be used for co-registration. Research has been done to automate multi-modality registration to remove the errors that arise during landmark based registration. Extensive research has been done for multi-modality registration of brain imaged through different *in vivo* imaging modalities like CT, PET, fMRI, SPECT, etc. [18][19][20]. But most automated registrations are between two *in vivo* modalities which do not have to deal with deformation caused to the image in *ex vivo* images. Comparing histology to MRI is still landmark based and done with manual visual decision making. Peter J. Hoskin et al. have studied the comparison between pimonidazole histology and BOLD MRI [21] and Stephanie B. Donaldson et al. have studied comparison of DCE MRI with pimonidazole histology [22]. Lejla Alic et al. have studied the registration of MRI and histology in tumors grown in rats. They have observed a decrease in tumor volume calculated from both the modalities after registration. This shows there is significant deformation in histology sectioning[23]. Maryana Alegro et al. have registered whole brain MRI images to histology [24].

This stresses on the need to study comparison between different modalities imaging hypoxia for a comprehensive and inclusive study. This research will investigate the ability of MRI agent GdDO3NI to depict clinically significant tumor hypoxia and show its efficacy in comparison to pimonidazole stained images. Establishing good correspondence in hypoxia intensity patterns after multi-modality registration of stacked histology and MRI should validate the use of GdDO3NI to study hypoxia. *In vivo* MRI based hypoxia imaging will become as significant as pimonidazole imaging which represents ground truth and hence eliminate the need for biopsy and staining for further studies.

# CHAPTER 2

# MATERIALS AND METHODS

## 2.1 INTER MODALITY REGISTRATION OF HISTOLOGY SECTIONS

DAPI is a fluorescent stain that binds strongly to adenine–thymine rich regions in DNA and hence DAPI images are used to delineate tumor tissue for analysis. The process of producing a final histology volume involved stacking and registration of DAPI stained images of 5 consecutive tumor sections, each of 30 μm thickness, obtained from fluorescence microscopy to produce a 3D stack of 150 μm thickness. The stack corresponds to a single T1 weighted gradient echo image of about 156 μm thickness. This was done through the iterative registration of the 5 consecutive DAPI images based on a quality metric like SSIM (Structural Similarity) Index.

The following procedures describe pre-processing done before registration of histology sections.

### 2.1.1 ROI Selection and Sampling

In intensity-based image registration it is essential to select out the region of interest in the image. The slide containing the tumor and any particles outside show up as different intensities in the histology image and have been carefully cropped out manually. For the next steps in the computational pipeline it was necessary to downsample the dataset to avoid running out of memory. Empirically a downsizing factor of 5 was found to give optimum registration time utilizing the 8GB RAM available. Hence all the input DAPI and PIMO images were resized accordingly.

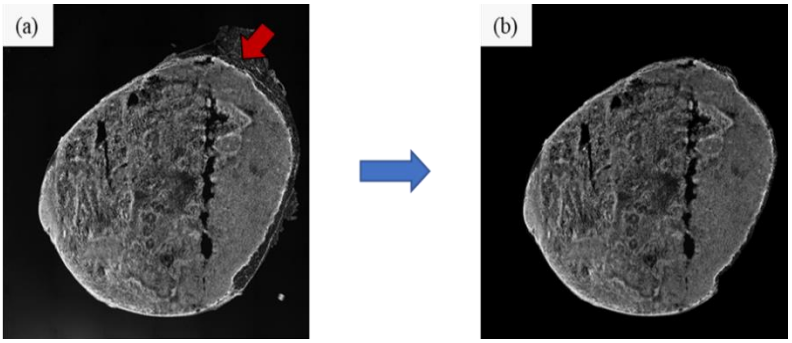


Figure 4 ROI selection to remove background noise

### 2.1.2 Histogram Equalization:

Histogram equalization is a contrast enhancement technique in image processing. Intensities in a series of images are better distributed after this adjustment. During acquisition of histology images, variation in lighting and unavoidable variations in staining intensity can cause intensity inconsistencies among the sections. This may cause one image to look brighter than another which in turn will give uneven registration results. This is fixed through a process called histogram equalization by use of a suitable MATLAB code. The code considers the histogram of the first image in the DAPI and PIMO stack as a global reference and matches the histogram ranges of the rest of the images to this reference.

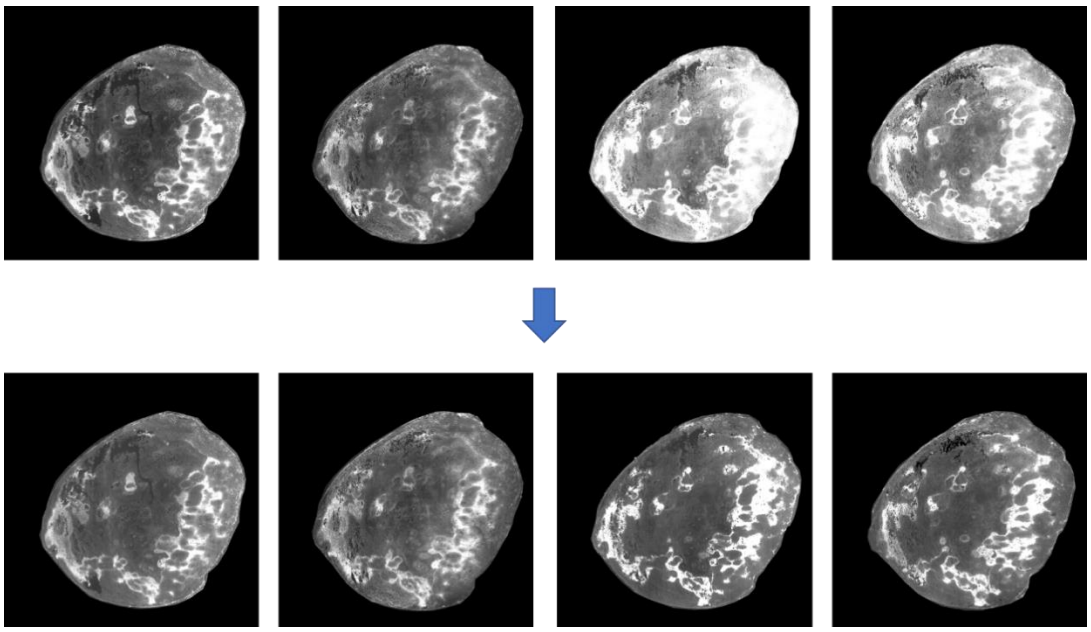

Figure 5 The first row shows a set of input images having intensity variations. The second row shows the same set after histogram equalization. The input image set now has consistent intensity range.

### 2.1.3 Thresholding of PIMO Images and PIMO Hypoxic Fraction

Thresholding is an effective segmentation technique to separate an image into a foreground and a background. The foreground shows information of interest and in this case highlights hypoxic regions. Hypoxic regions in PIMO images appear brighter (have higher intensity values) than normal non-hypoxic regions. A threshold value for hypoxic region is found by manually selecting 3 ROIs in normal regions and averaging the highest intensities found within each of these 3 regions. The thresholding is defined by the following equation:

$$I(x,y) = \begin{cases} f(x,y), & f(x,y) > T \\ 0, & f(x,y) \leq T \end{cases}$$

Where, T is the calculated threshold value, I(x,y) is the final thresholded image and f(x,y) is the intensity value of the pixel at coordinate (x,y). A threshold is found this way for each individual PIMO image. The average of these is considered as threshold used to calculate the PIMO hypoxic fraction of the stacked image. All pixel values above this threshold are considered hypoxic. The count is divided by the total number of pixels in the delineated tumor area to give the hypoxic fraction.

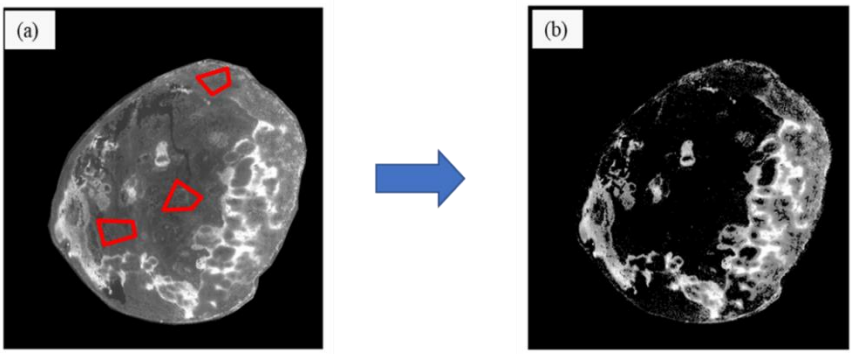


Figure 6 Input DAPI image before (a) and after (b) thresholding.

Description of MATLAB program for registration for each individual tumor:

The program reads the 5 input DAPI and 5 input PIMO images serially and stores to two separate stacks. The first DAPI image is stored as the fixed image and the second DAPI image is stored as the moving image. The moving image is then registered to the fixed image through the generation of a transform matrix using inbuilt functions imregister and imwarp. The transform is based on intensity difference and does rigid body translation and rotation. Both the fixed and moving images are referenced to fit a global reference frame based on intensity considering the pixel extent and image extent. Then the degree of translation and rotation in the global reference frame is found. After

the moving DAPI is registered to the fixed DAPI, the same registration transform is used to on the corresponding PIMO images. The two registered DAPI obtained from this process are stacked and averaged to obtain a final DAPI for comparison with the next DAPI. Next the registered DAPI from the previous step is stored as fixed image for the next registration step and the third DAPI from the original stack is stored as moving image. Registration is done again in the way described above. This loop continues till all the DAPI images are registered and all the corresponding PIMO images are registered. The resulting images are stacked and averaged for a final registered DAPI and PIMO image to represent all the 5 input images.

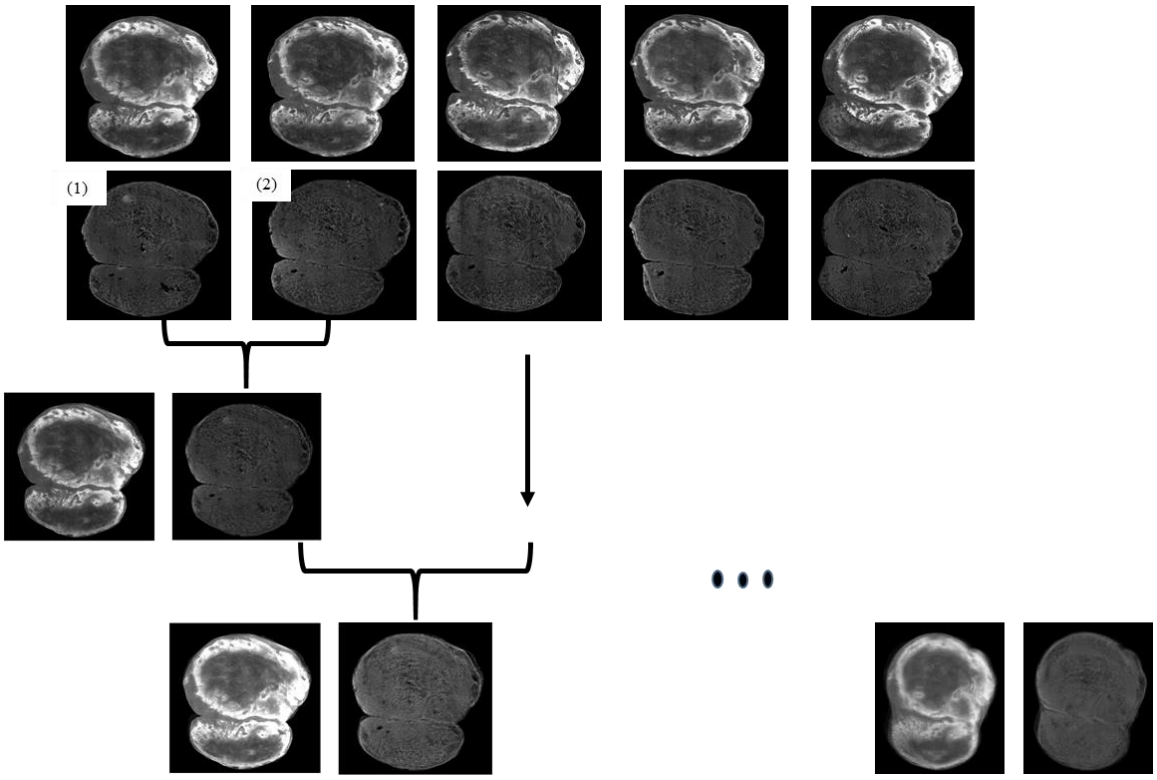

Figure 7 Representation of working algorithm for intra-modality registration. (1) is the first fixed image and (2) is the first moving image.

## 2.2 MULTI MODALITY IMAGE REGISTRATION

The registered IHC stack image was co-registered with a single T1 weighted gradient echo MRI slice of the same location (~156 μm thickness). This was performed through manual selection of corresponding boundary landmarks on DAPI stained image and MR image which generated an elastic B-splines transform. The resulting transform was applied to achieve the co-registration of pimonidazole and MR percentage enhancement image. The registration processes were done separately for each individual animal in MATLAB.

### 2.2.1 Pre-Processing before Co-Registration.

#### 2.2.1.1 MR Percentage Enhancement and Segmentation

The 3D gradient echo MR images obtained pre-GdDO3NI injection and 125 min post-injection are used to find a MR percentage enhancement image through a pre-developed MATLAB code. The pre-injection MR image is subtracted from MR image at 125 min post-injection. The result is divided by pre-injection image to remove baseline effect. One slice of the MR enhancement image is selected by visually comparing with the registered PIMO image. In-vivo MR images give a scanned image of the tumor along with the whole body of the mouse. After selection of the MR percentage enhancement slice, the corresponding T1 weighted gradient echo MR image obtained 60 min post-injection is segmented manually to select tumor region useful for comparison by the creation of a mask in MATLAB. This

involves careful selection of boundary to distinguish tumor from surrounding fat and muscle regions. The mask is then applied to corresponding MR percentage enhancement image.

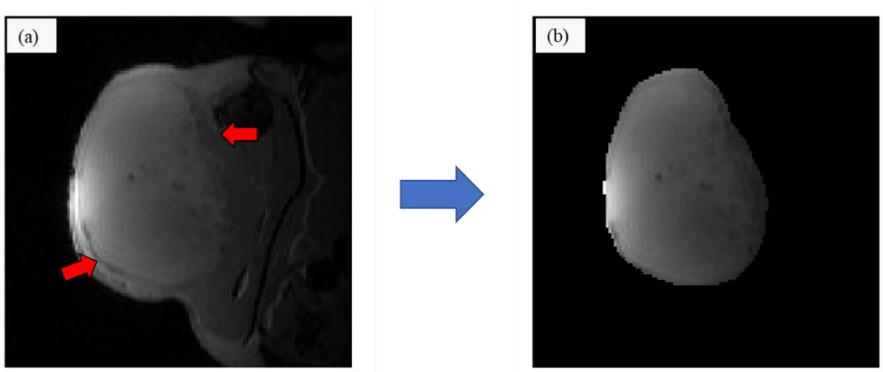


Figure 8 Input T1 weighted gradient echo MR image (b) after segmentation is done to keep tumor region of interest.

2.2.1.2 Thresholding and MR Hypoxic Fraction

Thresholding is done on the selected MR percentage enhancement image used for comparison with PIMO image. Hypoxic regions in MR percentage enhancement image appear brighter (have higher intensity values) than normal non-hypoxic regions. According to studies previously conducted in the lab [14], a threshold value of 10 percent over baseline is considered. This threshold is used to calculate the MR hypoxic fraction. All pixel values above this threshold are considered

hypoxic. The count is divided by the total number of pixels in the delineated tumor area to give the hypoxic fraction.

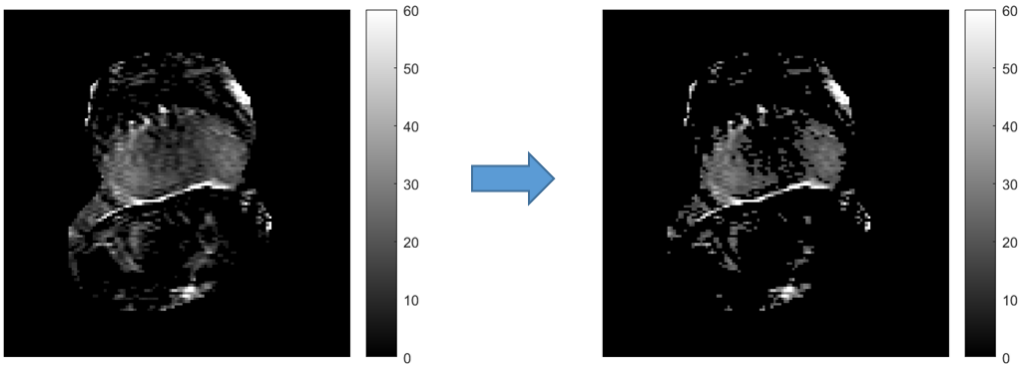


Figure 9 Input MR percentage enhancement image before (a) and after (b) thresholding.

2.2.1.3 Motion Correction

Motion artifact was detected between MR image acquired at 125 min post-gdDO3NI injection and MR image acquired before injection. This motion artifact can give rise to error in the MR percentage enhancement image which uses a subtraction of the two MR images. Since the motion occurs in 3 dimensions, the artifact is removed by 3D rigid body registration of the two gradient echo images using MATLAB code. The code references both the images according to a global frame of reference and matches the two images based on intensity difference to align both the images. Figure 11 depicts motion correction through checkerboard view. To show motion in 3D the xy, yz and zx planes are pictured individually which represent motion in z, x and y directions respectively. Boundary mismatch

(indicated by red arrow) in Figure 10 (a) is fixed in (b) after registration. Similarly, in Figure 11 the red arrows show changes in alignment after motion correction.

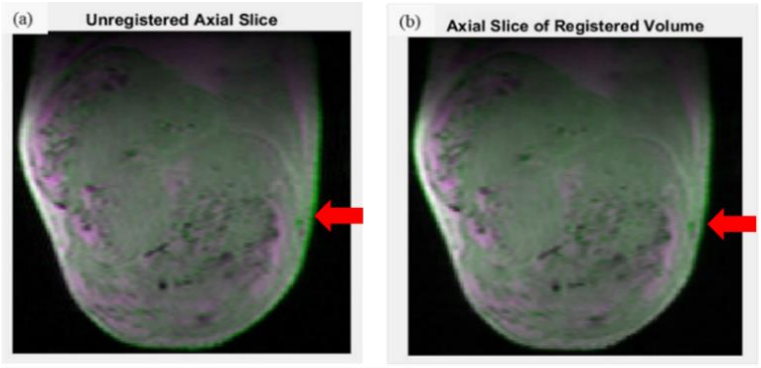


Figure 10 Overlay images of MR images at first and last time point of acquisition before (a) and after (b) motion correction for axial view orientation.

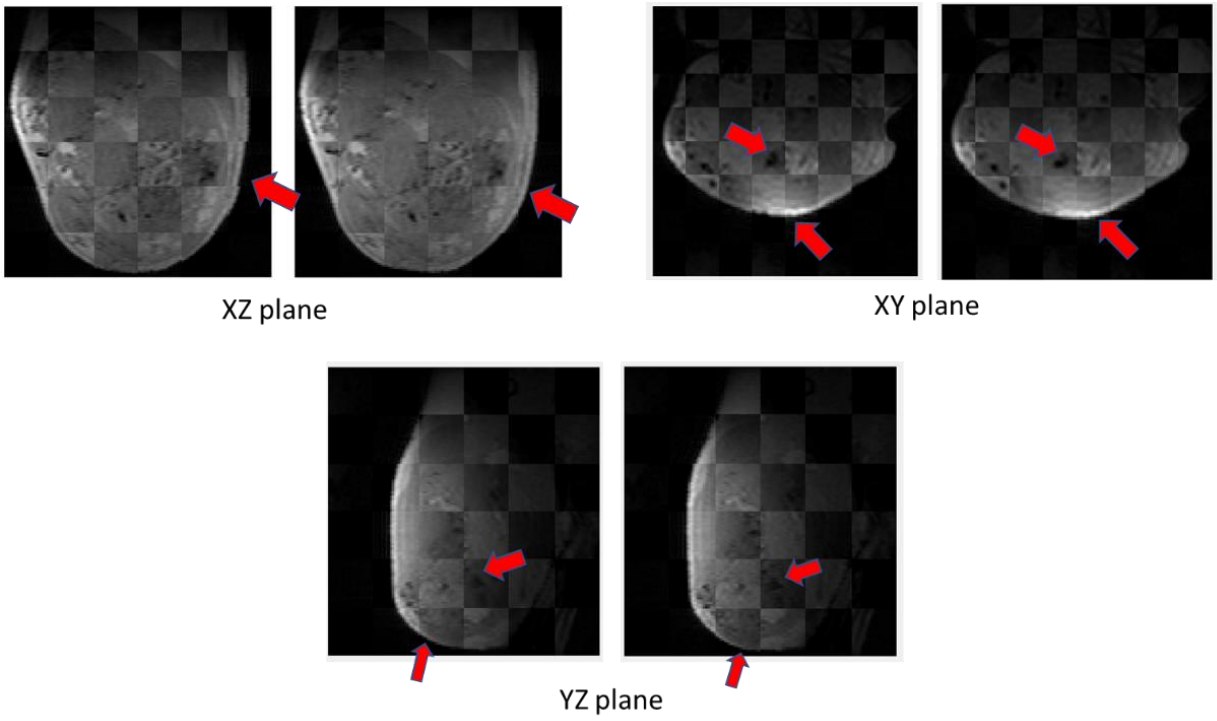

Figure 11 Checkerboard display of MR images of one tumor before (left-hand side image) and after (right-hand side image) motion correction shown in 3 directions to represent 3D motion.

### 2.2.2 Boundary Landmark Selection for Registration

A landmark in an image is a cognitive marker or reference point. Typically, image registration based on boundary landmarks focuses on matching the shapes in the two images. Boundary landmarks include sharp curves and edges in the over-all shape. To register PIMO to MR a careful selection of 6-10 corresponding points is done on each tumor. This can be seen Figure 12 as corresponding pairs of red and yellow dots on MR ROI image and DAPI ROI image. This is further used to generate transformation matrix for the co-registration.

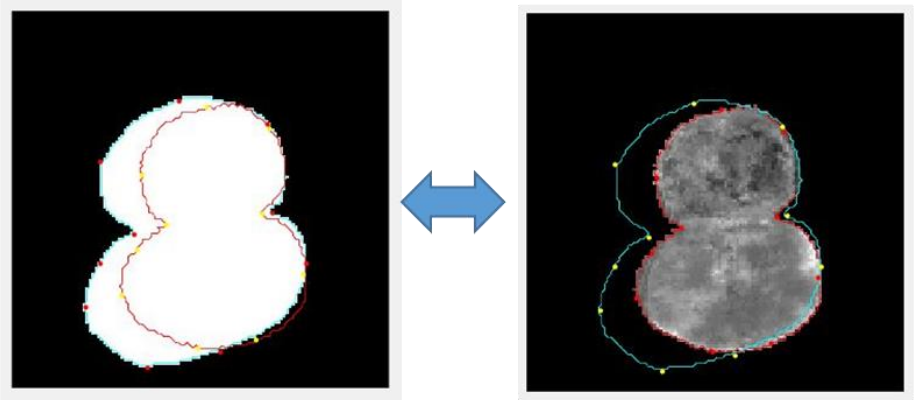

Figure 12 Landmark selection on MR ROI and DAPI ROI for correspondence

Description of MATLAB program for registration:

A MATLAB code developed previously in ProBE lab is used for the co-registration process. It uses MR percentage enhancement image to compare the intensity pattern

with input PIMO image. Corresponding T1 weighted gradient echo image at 60 min post-GdDO3NI injection and registered DAPI image are used as input to align the tumors for best co-registration results. Inbuilt function point_registration is used to create a 2D b-spline grid, which transforms the global space fit a set of points from moving image to a set of points on the fixed image. The function bspline_transform registers the two images based on the generated transform. This function is based on the algorithm written by D. Rueckert et al. [25].

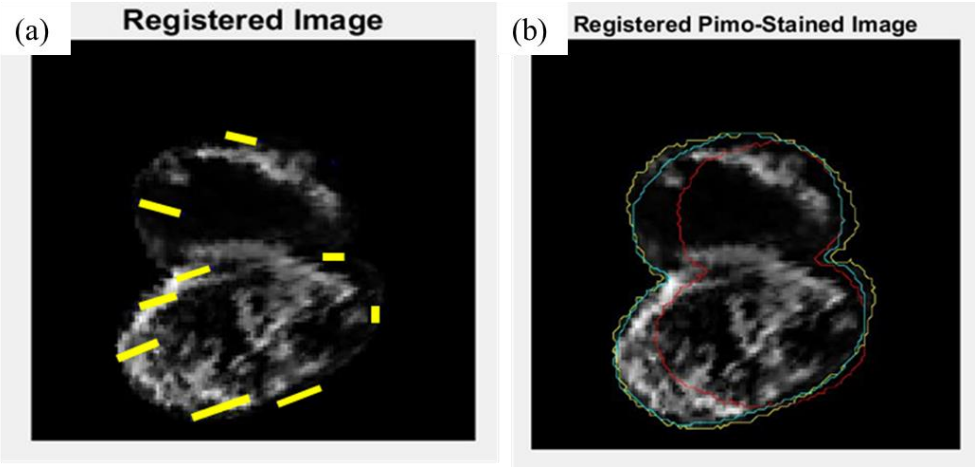


Figure 13 Yellow lines on (a) represent transformation followed after landmark selection to obtain a final registered PIMO image in (b).

### 2.2.3 Structural Similarity (SSIM) Index

MATLAB code is used to calculate the SSIM Index after co-registration. The SSIM is a qualitative statistic showing the similarity between two images. This index was first developed by Zhou Wang et al. [26]. It is based on the combination of three different measure: luminance comparison *l(x,y)*, contrast comparison *c(x,y)* and structural comparison *s(x,y)*. Luminance is estimated as the mean intensity, signal contrast is estimated by standard deviation and structural comparison is obtained after the signals

are normalized by their own standard deviations so that both signals have unit standard deviations. These comparisons are calculated locally from various windows on both the images measuring N*N size and is governed by the following final equation [26].

$$SSIM(x,y) = \frac{(2\mu_x\mu_y + c_1)(2\sigma_{xy} + c_2)}{(\mu_x{}^2 + \mu_y{}^2 + c_1)(\sigma_x{}^2 + \sigma_y{}^2 + c_2)}$$

Where, x and y are the two input images, $\mu_x$, $\mu_y$ are the means of y, $\sigma_x{}^2, \sigma_y{}^2$ are the variance of x and y, $\sigma_{xy}$ is the covariance of x and y, $c_1$ and $c_2$ are constants based on the dynamic range of pixel-values of the two images. This index lets us study the similarity in hypoxia intensity distribution depicted by both the imaging modalities.

### 2.2.4 Selection of Final MR Image Slice and Registered PIMO Image

One MR image thickness corresponds to combination of 5 consecutive histology sections. This requires a careful selection of MR image and input PIMO images to obtain the closest matching section and have proper registration. To achieve this, I have started by selecting an MR center slice and find various combinations of consecutive PIMO stacks. The MR center slice may also be changed to best match histology stack. Each PIMO stack is registered and co-registered with MRI to obtain similarity index value which indicates correspondence. The best corresponding result is kept for further analysis.

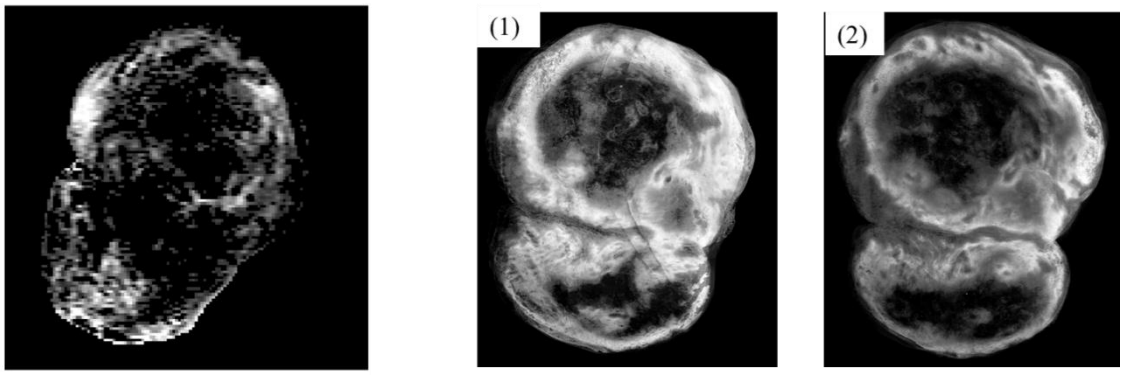


Figure 14 The first figure shows a selected a selected MR slice for one tumor and (1) and (2) show two different PIMO registered and stacked images to compare with MRI.

### 2.2.5 Coefficient of Determination and Root Mean Square Error

Coefficients of determination ($R^2$) is found for every tumor. One represents overall tumor hypoxia correlation and the other represents boundary $R^2$ to show correspondence of boundaries after co-registration. Hypoxic $R^2$ values are obtained from correlation between registered PIMO image and MR percentage image. For boundary $R^2$ value, boundaries are traced on binary masks of the final registered images using inbuilt MATLAB function bwtraceboundary. Correlation value is calculated from the obtained boundaries. Greater $R^2$ values represent better registration.

### 2.2.6 Statistical Analysis

The hypoxic fractions calculated from the MR image and the PIMO image were plotted using RStudio software. Linear regression line was plotted to view correlation. A 95% confidence interval area was plotted over the regression line to look for the possibility of outliers.

# CHAPTER 3

# RESULTS

Multiple co-registrations were done to find the matching center slices in both MR and histology set. This involved the combination of different sets of 5 consecutive histology sections to best align with a selection MR image. After the best images for comparison were determined the transform for correspondence is calculated based on manually selected landmarks, there. To minimize inconsistency due to human error, the co-registration process using the selected images was done multiple times and the best result with maximum visual alignment and SSIM index was selected for further hypoxia analysis.

## 3.1 Hypoxic Fraction Analysis

The hypoxic fractions obtained after registration were studied through correlation analysis with respect to PIMO hypoxic fraction. For half of the tumors hypoxic fractions represented by both modalities are similar. This means there is greater similarity in hypoxia imaged by the two different modalities. For one tumor, the MR hypoxic fraction and PIMO hypoxic fraction are widely different. This is an outlier in Figure 15 representing the scatter plot with regression line.

| | C1L0R0 | C1L0R1 | C6L0R0 | C5L0R1 | C7L0R0 | C8L0R1 |
|---|---|---|---|---|---|---|
| **MR Hypoxic fraction** | 0.84 | 0.4179 | 0.5325 | 0.4396 | 0.4391 | 0.4239 |
| **Pimo Hypoxic fraction** | 0.23 | 0.2716 | 0.3741 | 0.444 | 0.1934 | 0.1284 |

Table 1 Comparison of hypoxic fractions post registration

A 95% confidence interval range is also plotted along with the regression line. The outlier is seen to be outside the confidence interval range. The $R^2$ value obtained is 0.237. Since, one data point lies outside confidence interval, it was removed from the dataset and correlation study was done again. As seen in Figure, after exclusion of outlier the remaining 5 tumors lie within 95% confidence interval range. The $R^2$ value obtained is 0.486 showing a great increase with respect to original correlation study.

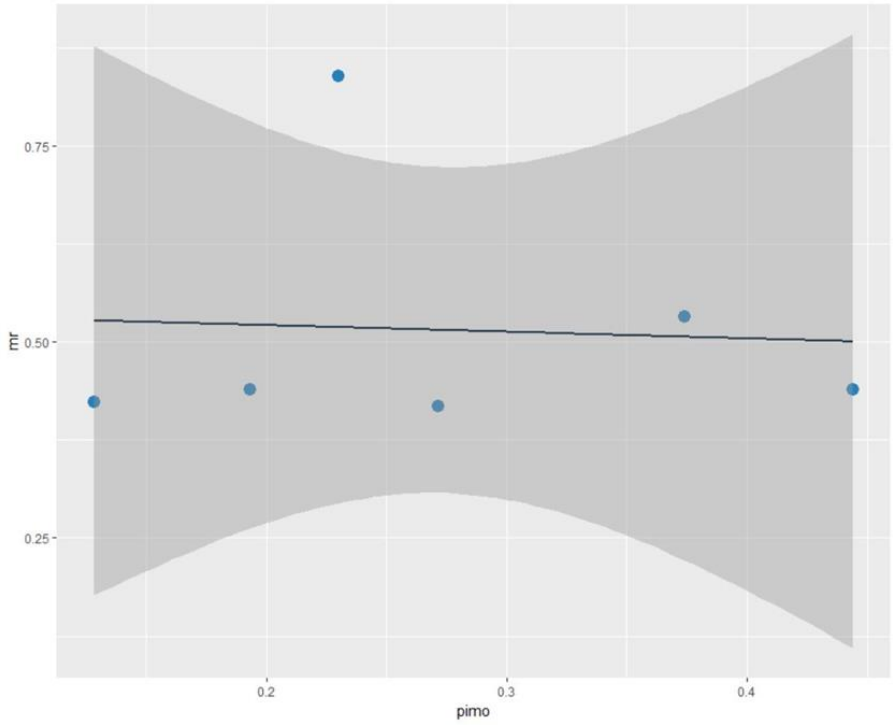


Figure 15 Scatter plot for hypoxia fractions for all 6 tumors. X axis represents PIMO hypoxic fraction and Y axis represents MR hypoxic fraction. Shaded area represents 95% confidence interval range.

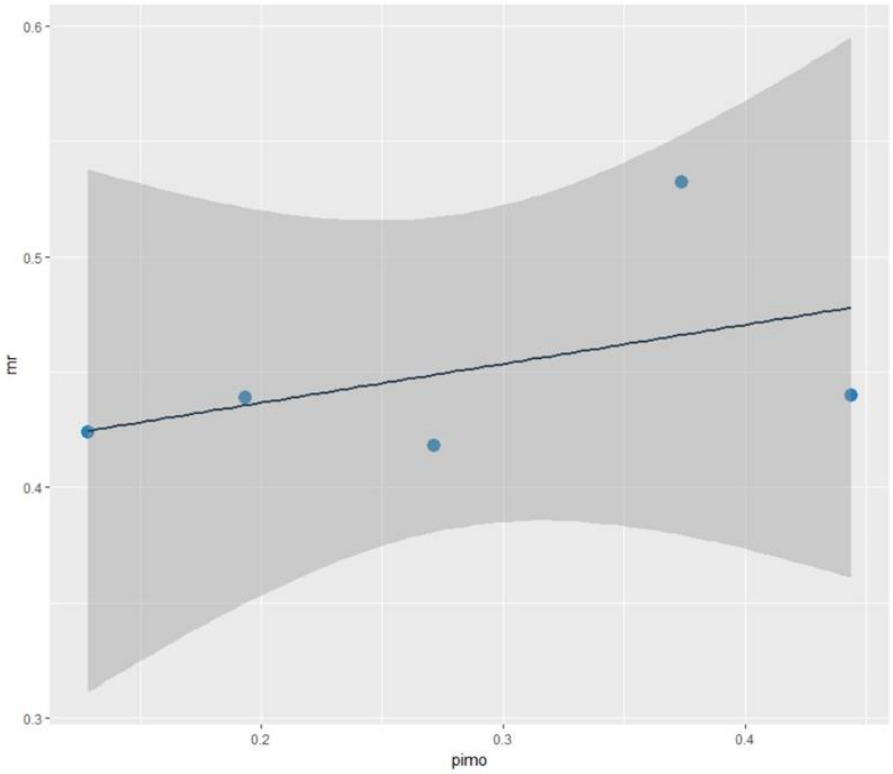


Figure 16 Scatter plot for hypoxia fractions for all 5 tumors (excluding oulier). X axis represents PIMO hypoxic fraction and Y axis represents MR hypoxic fraction. Shaded area represents 95% confidence interval range.

### 3.2 Comparison of Registration Metrics

Image similarity index after the co-registration was found to be greater than 0.5 for 5 of the animals suggesting good correlation. $R^2$ values were calculated for tumor boundaries. All the tumors showed a high boundary correlation value of $R^2$ greater than 0.8. This is an indicator of proper selection of landmarks for registration and higher accuracy of registration transform.

| | C1L0R0 | C1L0R1 | C6L0R0 | C5L0R1 | C7L0R0 | C8L0R1 |
|---|---|---|---|---|---|---|
| **Boundary $R^2$** | 0.919 | 0.917 | 0.889 | 0.8605 | 0.8610 | 0.8539 |
| **Similarity Index** | 0.7104 | 0.7397 | 0.57 | 0.45 | 0.644 | 0.6117 |

Table 2 Comparison of metrics obtained from the multi-modality registration process for the six tumor-bearing animals.

A similar trend between calculated boundary $R^2$ and similarity index can be observed. The tumor corresponding to highest $R^2$ has highest SSIM and vice-versa.

### 3.3 Visualization of Intra Modality Registration

The registered and stacked histology sections are visualized using a 3D volume viewer in ImageJ to check boundary outline of registered stack. If boundary continuation looks inconsistent then the registration process is repeated with modification to registration optimizer and iteration parameters. This is done we see consistent boundary outline and a definitive consistency in internal structure intensity.

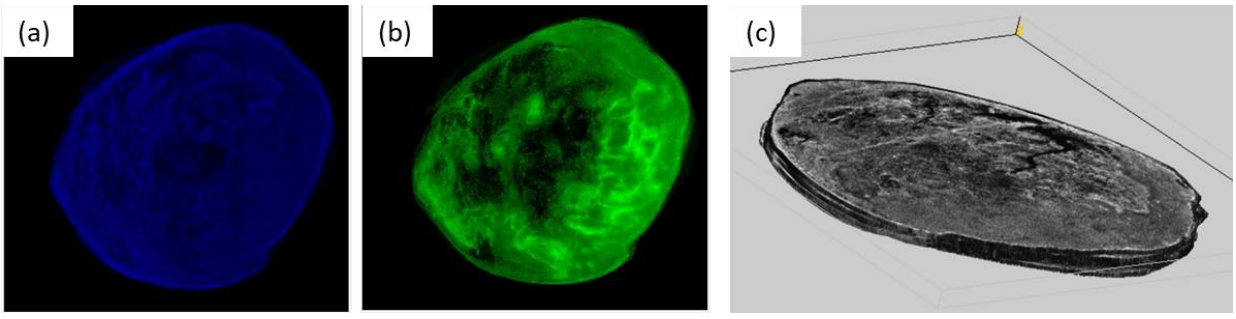


Figure 17 Intra-modality registration results. (a) Registered DAPI stained image stack and (b) Registered pimonidazole image stack for the first animal. 3D visualization of

registered DAPI stack shown in grayscale in (c) shows consistent boundary outline between the histology sections.

### 3.4 Visualization of Inter Modality Registration

The co-registration is studied visually to check for alignment. Alignment and boundary correspondence is also verified with the help of checkerboard display. Checkerboard display overlays the two images and make comparison of internal intensity patterns easy.

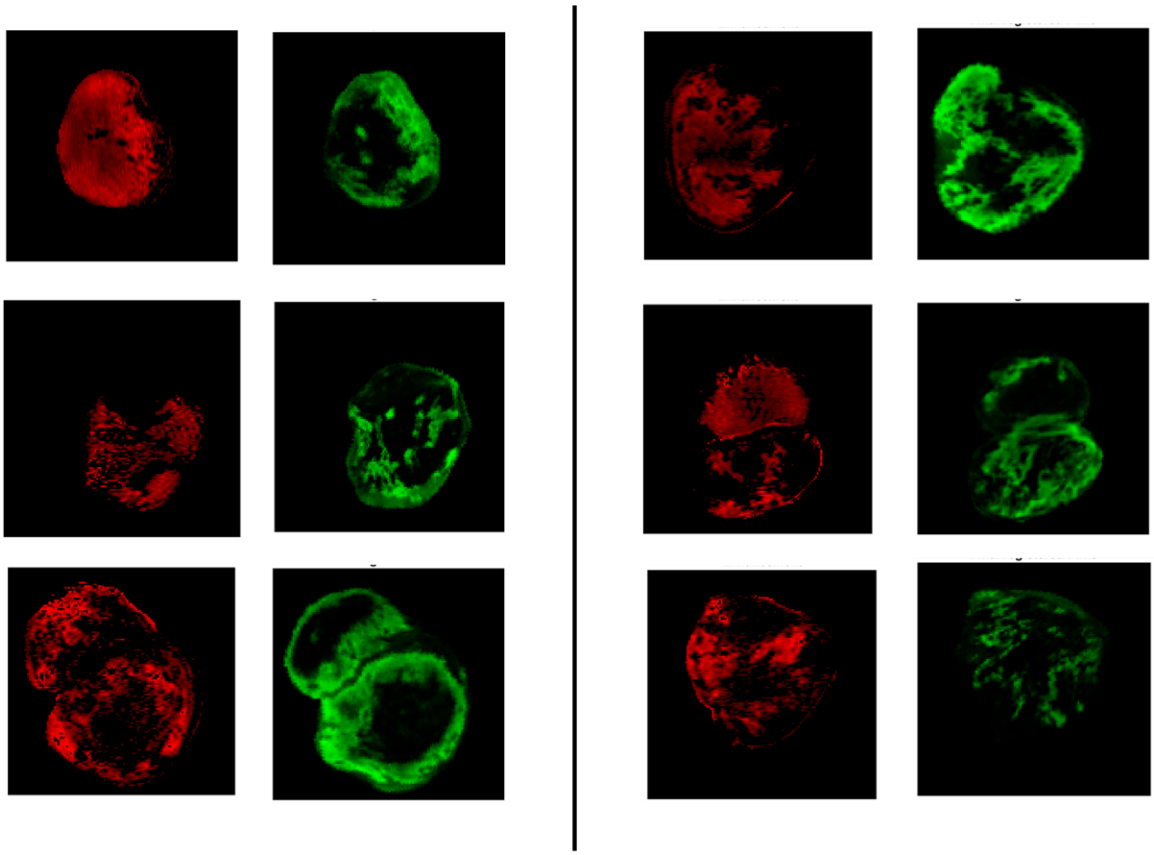

Figure 18 Representation of inter-modality registration of MR and Histology for the six tumors. First column shows thresholded MR percentage enhancement image and second column shows pimonidazole image generated after co-registration.

To show efficiency of co-registration the input ROI boundaries and the final boundary obtained after co-registration are plotted on the final registered PIMO image. In each case the green boundary represents ROI of input MR image, the red boundary represents ROI of input DAPI and the yellow boundary represents ROI of final registered image. From Figure 19 it can be seen all the tumors there is high boundary correspondence after registration.

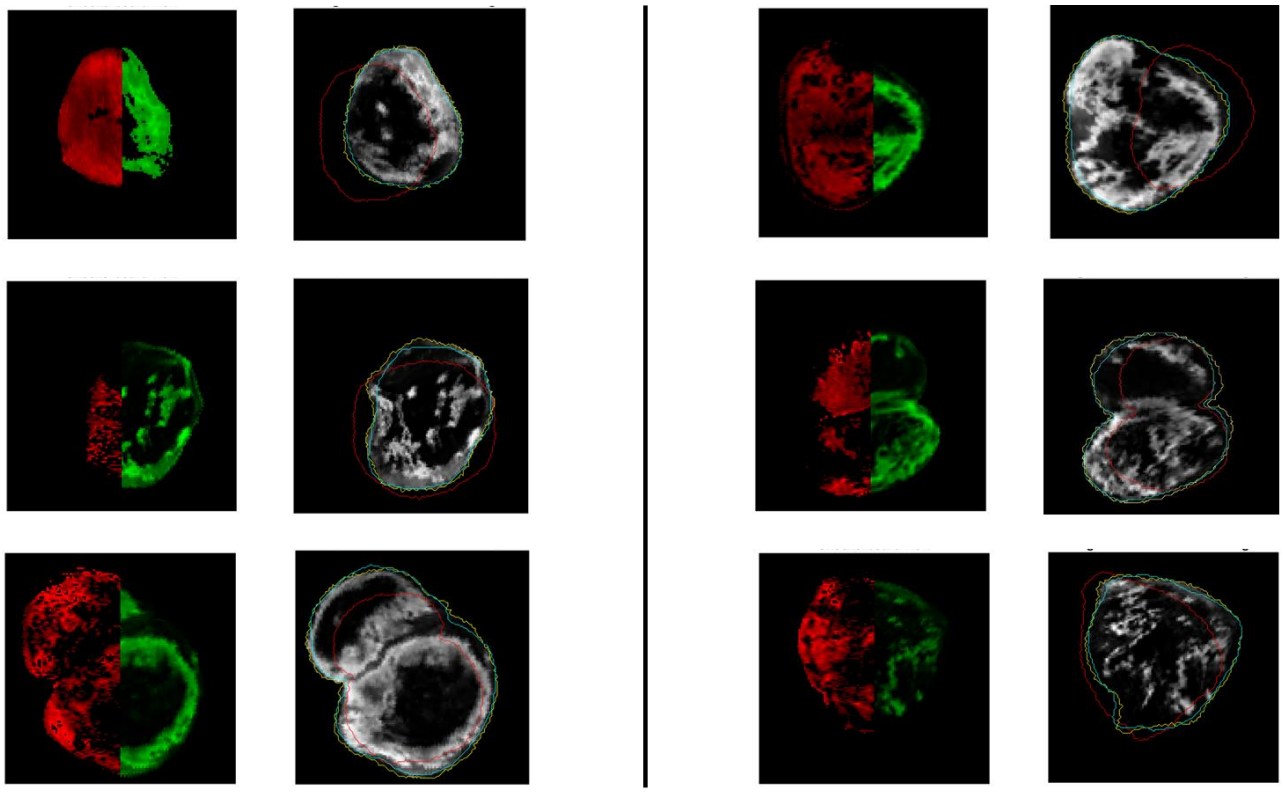

Figure 19 Left-hand image shows checkerboard view after co-registration for the six tumors. Right-hand image in each case shows ROI boundaries on the final registered PIMO image.

In three of the cases a strong correspondence can be seen visually in the internal distribution of hypoxia. For a few tumors internal intensity correspondence is low and should be further investigated. The RMSE values for the co-registration of all the animals were found to be low further suggesting better correspondence and more accuracy.

## CONCLUSION

Non-rigid registration is essential in the process of registering histology sections. Matching of histological PIMO stained sections to MR images of tumors is facilitated by using a multi-step registration process. The six tumors were successfully co-registered and hypoxia patterns were studied. All the tumors show good boundary correlation, however, there is mismatch in internal patterns in two of the tumors. This may be due to distortion caused by sectioning and staining. Good boundary correlation and high correlation value for PIMO hypoxic fraction and MR hypoxic fraction indicate a high similarity in hypoxia imaging by pimonidazole and MR agent GdDO3NI. This is further supported by similarity index calculation which is high for 5 of the tumors. Thus, validating GdDO3NI based MRI as a convenient *in vivo* hypoxia imaging method. This will help future studies in saving time and resources by not having to do histology and will make detection and diagnosis based on hypoxia faster.

## FUTURE WORK

For a highly accurate co-registration with good correspondence in internal intensities, a more extensive study is needed. In this regard, there are several possible procedures which could be implemented to further increase the robustness and accuracy of the technique within a reasonable processing time. For example, using the full color range of the histology images could help automatic segmentation. Acquiring images with a stereotactic marker system12 could facilitate the rigid registration of images. This has been seen to speed up the registrations and make manual annotations easier [27]. The use of contrast agent to alter the tumor structural detail and highlight different orientation should be considered as well. Though not extremely promising due to variations arising from sectioning artifacts, completely automated co-registration instead of manual landmark selection should be considered too.

REFERENCES


[1] G. 2015 D. and I. I. and P. GBD 2015 Disease and Injury Incidence and Prevalence Collaborators, “Global, regional, and national incidence, prevalence, and years lived with disability for 310 diseases and injuries, 1990-2015: a systematic analysis for the Global Burden of Disease Study 2015.,” *Lancet (London, England)*, vol. 388, no. 10053, pp. 1545–1602, 2016.

[2] P. Vaupel and L. Harrison, “Tumor hypoxia: causative factors, compensatory mechanisms, and cellular response.,” *Oncologist*, vol. 9 Suppl 5, no. suppl 5, pp. 4–9, 2004.

[3] H. HARADA, “How Can We Overcome Tumor Hypoxia in Radiation Therapy?,” *J. Radiat. Res.*, vol. 52, no. 5, pp. 545–556, 2011.

[4] J. M. Brown, “Tumor Hypoxia in Cancer Therapy,” *Methods Enzymol.*, vol. 435, pp. 295–321, Jan. 2007.

[5] R. E. Durand, “The influence of microenvironmental factors during cancer therapy,” *In Vivo (Brooklyn).*, vol. 8, no. 5, pp. 691–702, 1994.

[6] K. M. Comerford, T. J. Wallace, J. Karhausen, N. A. Louis, M. C. Montalto, and S. P. Colgan, “Hypoxia-inducible factor-1-dependent regulation of the multidrug resistance (MDR1) gene,” *Cancer Res.*, vol. 62, no. 12, pp. 3387–3394, 2002.

[7] P. Vaupel and A. Mayer, “The Clinical Importance of Assessing Tumor Hypoxia: Relationship of Tumor Hypoxia to Prognosis and Therapeutic Opportunities,” *Antioxid. Redox Signal.*, vol. 22, no. 10, pp. 878–880, 2015.

[8] J. M. Brown, “Selective Radiosensitization of the Hypoxic Cells of Mouse Tumors with the Nitroimidazoles Metronidazole and Ro 7-0582,” *Radiat. Res.*, vol. 64, no. 3, pp. 633–647, 1975.

[9] W. J. G. Oyen, J. H. A. M. Kaanders, and J. Bussink, “Molecular imaging of hypoxia,” *Quarterly Journal of Nuclear Medicine and Molecular Imaging*, vol. 57, no. 3, pp. 217–218, 2013.

[10] P. K. Gulaka, F. Rojas-Quijano, Z. Kovacs, R. P. Mason, A. D. Sherry, and V. D.

Kodibagkar, “GdDO3NI, a nitroimidazole-based T1 MRI contrast agent for imaging tumor hypoxia in vivo,” *J Biol Inorg Chem*, vol. 19, no. 2, pp. 271–279, 2014.

[11] M. A. Varia *et al.*, “Pimonidazole: A novel hypoxia marker for complementary study of tumor hypoxia and cell proliferation in cervical carcinoma,” *Gynecol. Oncol.*, vol. 71, no. 2, pp. 270–277, 1998.

[12] L. A. Huxham, A. H. Kyle, J. H. E. Baker, K. L. McNicol, and A. I. Minchinton, “Tirapazamine causes vascular dysfunction in HCT-116 tumour xenografts,” *Radiother. Oncol.*, vol. 78, no. 2, pp. 138–145, 2006.

[13] L. J. Bains, J. H. E. Baker, A. H. Kyle, A. I. Minchinton, and S. A. Reinsberg, “Detecting Vascular-Targeting Effects of the Hypoxic Cytotoxin Tirapazamine in Tumor Xenografts Using Magnetic Resonance Imaging,” *Int. J. Radiat. Oncol. Biol. Phys.*, vol. 74, no. 3, pp. 957–965, 2009.

[14] S. Agarwal, R. Vidya Shankar, L. J. Inge, J. Smaill, A. V Patterson, and V. Kodibagkar, “Mri assessment of changes in tumor oxygenation post hypoxia-targeted therapy,” *Mol. Imaging Biol.*, vol. 17, no. 1, 2015.

[15] D. Pilutti, M. Buchert, and S. Hadjidemetriou, “Registration of abdominal tumor DCE-MRI data based on deconvolution of joint statistics,” in *Proceedings of the Annual International Conference of the IEEE Engineering in Medicine and Biology Society, EMBS*, 2013, pp. 2611–2614.

[16] L. S. Taylor *et al.*, “Three-dimensional registration of prostate images from histology and ultrasound,” *Ultrasound Med. Biol.*, vol. 30, no. 2, pp. 161–168, 2004.

[17] Y. Zhan, Y. Ou, M. Feldman, J. Tomaszeweski, C. Davatzikos, and D. Shen, “Registering Histologic and MR Images of Prostate for Image-based Cancer Detection,” *Acad. Radiol.*, vol. 14, no. 11, pp. 1367–1381, 2007.

[18] P. J. Slomka and R. P. Baum, “Multimodality image registration with software: state-of-the-art,” *Eur. J. Nucl. Med. Mol. Imaging*, vol. 36, no. 1, p. 44, 2008.

[19] A. W. Toga and P. M. Thompson, “The role of image registration in brain mapping,” *Image Vis. Comput.*, vol. 19, no. 1–2, pp. 3–24, 2001.

[20] C. Wang, J. J. Pahl, and R. E. Hogue, “A method for co-registering three-dimensional multi-modality brain images.,” *Comput. Methods Programs Biomed.*, vol. 44, no. 2, pp. 131–40, 1994.

[21] P. J. Hoskin *et al.*, “Hypoxia in Prostate Cancer: Correlation of BOLD-MRI With Pimonidazole Immunohistochemistry-Initial Observations,” *Int. J. Radiat. Oncol. Biol. Phys.*, vol. 68, no. 4, pp. 1065–1071, 2007.

[22] S. B. Donaldson *et al.*, “Perfusion estimated with rapid dynamic contrast-enhanced magnetic resonance imaging correlates inversely with vascular endothelial growth factor expression and pimonidazole staining in head-and-neck cancer: A pilot study,” *Int. J. Radiat. Oncol. Biol. Phys.*, vol. 81, no. 4, pp. 1176–1183, 2011.

[23] L. Alic *et al.*, “Facilitating tumor functional assessment by spatially relating 3D tumor histology and In Vivo MRI: Image registration approach,” *PLoS One*, vol. 6, no. 8, 2011.

[24] M. Alegro *et al.*, “Multimodal Whole Brain Registration: MRI and High Resolution Histology,” in *IEEE Computer Society Conference on Computer Vision and Pattern Recognition Workshops*, 2016, pp. 634–642.

[25] D. Rueckert et al., “Nonrigid registration using free-form deformations: application to breast MR images.,” *IEEE Trans. Med. Imag.*, vol. 18, no. 8, pp. 712–21, 1999.

[26] Z. Wang, A. C. Bovik, H. R. Sheikh, and E. P. Simoncelli, “Image quality assessment: From error visibility to structural similarity,” *IEEE Trans. Image Process.*, vol. 13, no. 4, pp. 600–612, 2004.

[27] L. Alic *et al.*, “Multi-modal image registration : matching MRI with histology,” *Imaging*, vol. 7626, pp. 1–9, 2010.